EXPERIMENTAL AND ANALYTICAL STUDY OF QUASI-STEADY MPD CHANNEL FLOW

K. Mitsuo*, H. Tahara**, H. Okutani*,
Y. Kagaya+ and T. Yoshikawa++

Faculty of Engineering Science, Osaka University
Toyonaka, Osaka, Japan

Abstract

Plasma diagnostic measurement and numerical analysis in quasi-steady coaxial magnetoplasmadynamic (MPD) channels were made to understand blowing acceleration, i.e., one-dimensional flowfield. Current distributions on the electrodes, electron temperatures and electron number densities in the channels were measured. In addition, to establish a scaling law, current distributions were measured with varying different channel length. For Ar, the measured current fractions on the anode intensively increased near the exit. However, those on the cathode gradually increased downstream, and a slight current concentration was observed near the inlet at high magnetic Reynolds numbers. Furthermore, it was found, from the experimental results with the different length MPD channels, that the profiles of current distributions are roughly determined by Rm, and the scaling law was confirmed as predicted from the one dimensional flowfield analysis. The electron temperatures were axially kept about 12000K and slightly increased near the inlet and outlet. The electron number densities increased near the exit, and the characteristics corresponded to the current distributions. The experimental results agreed roughly with the analyzed ones. Accordingly, it is expected from the axial profiles of Lorentz forces and the calculated plasma velocities that there are two acceleration zones near the inlet and outlet at high Rm.

Introduction

The magnetoplasmadynamic (MPD) arcjet is a promising thruster which is developed for exploration missions to the moon and Mars, and for raising orbits of large space structures. In Japan, the experimental MPD arcjet onboad SFU(Space-Flyer-Unit) was tested in 1995 for practical use in the future.[1] The MPD arcjet utilizes principally electromagnetic force, i.e, Lorentz force j×B, which is generated by interaction between discharge current and magnetic field azimuthally induced by the discharge current. Various propellants, such as light gases of H_2 and Li, heavy gases of Ar and Xe, and waste ones in space stations etc., can be used, because the thrust depends only on the discharge current and does not basically on propellant species for electromagnetic acceleration. However, in an MPD chamber, complicated chemical reactions involving dissociation and ionization are expected to occur together with the acceleration processes. Furthermore, for acceleration theory of MPD arcjets, there exist two components of electromagnetic force, i.e., the blowing force and pumping force. These forces generate a complicated flowfield in a discharge chamber. Consequently, it has been recognized that the performance characteristics on the discharge voltage, thrust efficiency and electrode erosion depend on propellant species and electrode geometry.[2-7]

Many researchers have investigated experimentally the flowfield in MPD discharge chambers. However, the plasma acceleration processes were not clarified in detail. To understand the plasma acceleration processes, it is necessary to gather more information of the flowfield in MPD chambers.

In Osaka University, a new research program for understanding of an MPD arcjet acceleration mechanism was started in 1991. It was based on an unique concept that two electromagnetic forces , i.e., the blowing and pumping forces should be independently examined with two different simple discharge chambers. By using simple chamber configurations, plasma diagnostic measurements of MPD chambers can be easily conducted, and unknown information on the plasma acceleration mechanism can be obtained.[8,9]

In the present study, plasma diagnostic measurement and flowfield analysis in quasi-steady MPD channels, realizing only electromagnetic blowing acceleration, i.e., a one dimensional flowfield, are carried out to understand plasma features and acceleration processes. The current distributions on the electrodes were examined using a segmented anode and cathode, and the different length channels (100 mm, 200 mm) were used in order to understand a scaling law. In addition, optical measurement was conducted, and the electron temperatures and the electron number densities were estimated.

Furthermore, the numerical analysis with one-

---

*Graduate Student of Osaka University
**Associate Professor, Member JSASS/AIAA
+Assistant Engineer, Member JSASS
++Professor, Member JSASS/AIAA

dimensional flowfield was conducted in order to compare experimental results with calculated ones and understand plasma acceleration processes in an MPD channel. In this calculation, two temperature (electron temperature and heavy particle temperature) and non-equilibrium chemical reactions were considered.

Experimental Apparatus and Operational Condition

The coaxial MPD channel (MC-Ⅱ) shown in Fig.1 was designed in order to both experimentally and analytically investigate the MPD channel flow. The straight anode made of copper is 200 mm long and 50 mm in inner diameter, and the rod cathode made of molybdenum is 200 mm long × 25 mm in diameter. The anode is divided axially into 10 anode parts, each of which is electrically insulated to one another. In measurement of current distributions on the electrode, the cathode is also divided into ten cathode parts. On the other hand, in the experiment with the short length channel, the channel length is shortened to 100 mm long, and both anode and cathode are divided axially into 5 segments, respectively. To distinguish the long MPD channel from the short one, they are named MC-Ⅱ-α, MC-Ⅱ-β, respectively. They are not provided with floating electrodes, and gas is injected uniformly from the upstream end of the discharge chamber. Furthermore, the downstream end of the electrodes are provided with insulators which prevent current from concentrating on their surfaces of the edge of MPD channels and from spreading out of the discharge chamber; that is, they are covered with insulators as pumping force does not act in MPD channels. Gases are injected from 4 gas ports into the discharge chamber through a fast acting valve (FAV) fed from a high pressure reservoir. The rise time and the width of the gas pulse, measured with a fast ionization gauge, are 0.5 and 6 msec, respectively. The mass flow rates are controlled by the adjustment of the reservoir pressure and orifice diameter of the FAV. Argon and Nitrogen are used as propellants. However, in this paper, results for argon is discussed, and those for nitrogen is reported in ref.8.

The main power-supplying pulse forming network, which is capable of storing 62 kJ at 8 kV, delivers a single non-reversing quasi-steady current of maximum 27 kA with a pulse width of 0.6 msec. A vacuum tank 0.6 m in diameter × 5.75 m in length, where the MPD channel is fired, is evacuated to some 10^{-2} Pa prior to each discharge. Discharge current is measured with a Rogowski coil calibrated with a known shunt resistance. Voltage measurement is performed with a current probe (Iwatsu CP-502), which detects the small current bled through a known resistor (10k Ω) between the electrodes.

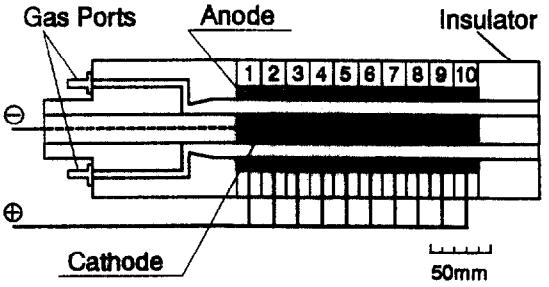

Fig.1 Cross section of MPD channel (MC-Ⅱ).

In the present study, the magnetic Reynolds number Rm, characterized the flowfield, is defined as follows.

$$Rm = \sigma\mu_0 U_{ref} L, \qquad U_{ref} = AB_0^{\,2} / 2\mu_0 \dot{m}$$

where σ is electrical conductivity, μ_0 permeability in vacuum, U_{ref} reference velocity, L the channel length, B_0 the magnetic field at the inlet, A the area of the cross section and $\dot{m}$ mass flow rate.

The discharge current is fixed at 8 kA, and Rm was changed with mass flow rates, in which the electrical conductivity was estimated from the numerical analysis. The mass flow rate at Rm=5 is set up at a corresponding critical current of about 8 kA, which is derived theoretically from the role of minimum input power or Alfvén's critical ionization velocity.[10]

Table.1 Mass Flow Rate and Electrical Conductivity for Ar.

Rm	Mass Flow Rates (g/s)	Electrical Conductivity (moh/m)
2	1.015	2000
5	0.481	2350
10	0.254	2500
20	0.152	3000

Measurement of current fractions on the electrodes

The current entering each electrode segment is measured with a Rogowski coil calibrated with a known shunt resistance in order to examine current fractions on electrodes, that is, to infer the current pattern in the interelectrode region. In this experiment, both the long and the short length MPD channel (MC-Ⅱ-α, β) were used for understanding the scaling law, and their duration times were 1.2 msec and 0.6 msec, respectively. Current waveforms were measured in the steady-state condition except the transitional state at start of the discharge.

Emission spectroscopic measurement

Emission spectroscopic measurement is conducted as reliable plasma diagnostic in MPD discharge chambers. Light comes from the plasma

through a slit 1 mm in width between anode segments. The emission is collected by a lens and introduced into a 0.5-m monochrometer through an optical fiber. The monochrometer of diffraction-grating-type HAMAMATSU C5095 is provided with 150- and 2,400-grooves/mm grating plates, an image intensifier and a 1024-channel diode array detector, achieving spectral resolutions of 0.8 and 0.05 nm, respectively, per detector channel. The electron temperature is determined using a relative intensity method of spectral lines, i.e., by means of Boltzmann plotting with Ar Ⅱ or N Ⅱ spectral lines. The electron density is estimated from the stark width of hydrogen H β line (486.13 nm), in which a mixture of argon or nitrogen and a few percent seed hydrogen is used. Light-of-sight measurement is conducted, and horizontally-average physical properties are calculated directly from the measured horizontally-integrated spectral intensities; i.e., Abel transformations are not carried out.

In optical measurement, MPD plasma was examined in a steady-state condition by avoiding transitional phenomena near the start and end of the discharge. The discharge duration time is 1.2 msec, and the emission from plasma is measured for a period of 0.6 msec after 0.4 msec from the discharge ignition. The timing is controlled with a gate of the image intensifier, which can open or close the entrance to the array detector. The emission was measured at seven axial points at the middle of the interelectrode.

Experimental Results and Discussion

Current fractions

Figure 2 shows current fractions for Ar on the electrodes with the long MPD channel (MC-Ⅱ-α). The current fractions on the anode intensively increase downstream; however, those on the cathode gradually increase. For the current fractions at high magnetic Reynolds number, there exists a slight current concentration near the inlet; furthermore, current in the upper stream region of the channel decrease in quantity as Rm is high. This is expected because back-EMF is large at high Rm. Besides, it is expected that a little axial current flows in the channel, since the current pattern on the anode slightly different from that on the cathode.

Lorentz forces

The Lorentz forces $j_r \times B_\theta$ inferred from the current fractions at Rm=2～20 is shown in Fig.3, in which j_r is the average between the anode and the cathode current fractions, and the azimuthal magnetic field B_θ at the center of the interelectrode is calculated with the current fractions into the cathode. Since the Lorentz forces for Ar at Rm=5～20 are very high near the inlet and outlet, it is expected that plasma is accelerated in these zones. Furthermore, Lorentz force at the exit of the channel at Rm=20 is about twice as large as that at Rm=5.

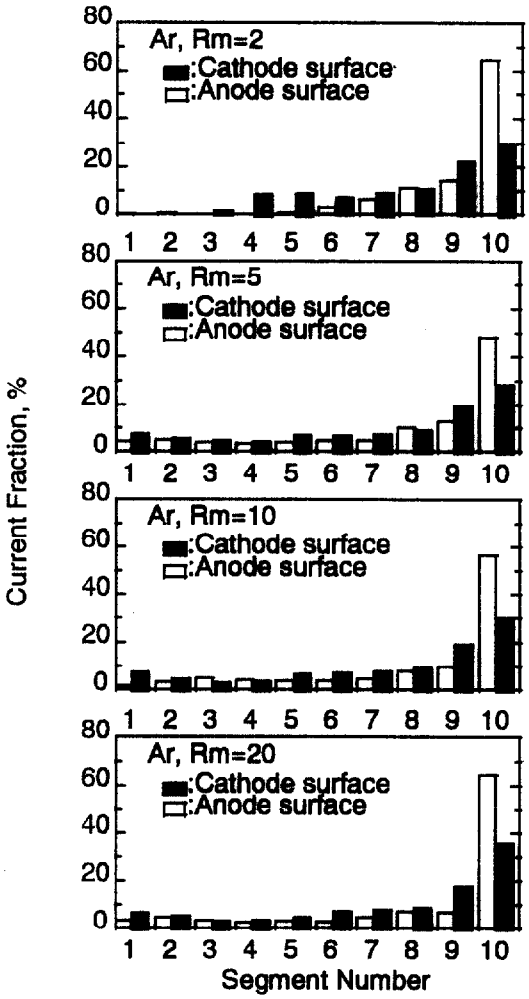

Fig. 2 Current fractions on electrodes for Ar at Rm=2～20.

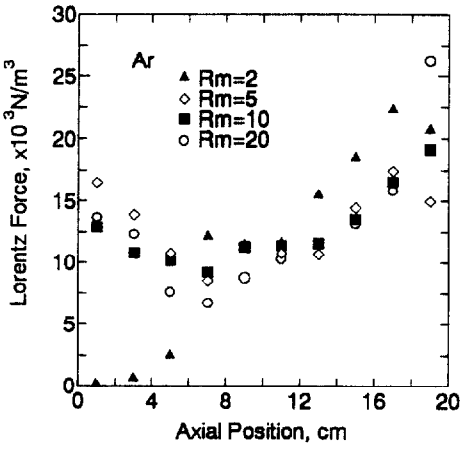

Fig.3 Lorentz forces evaluated from measured current fractions for Ar at Rm=2～20.

Electron temperature and electron number density

The axial variations of electron temperatures and electron number densities for Ar are shown in Figs.4 and 5. The electron temperatures are kept about 12000 K in the intermediate region, and they slightly rise near the inlet and outlet. The characteristics roughly corresponded to the current distributions on the electrodes, because electron temperatures strongly depend on Joule heating. The electron number densities are almost constant from upstream end to the middle point of the channel and increase near the exit. They range from 1.0×10^{20} to 5.0×10^{20} m^{-3}. The profiles of electron temperatures and electron number densities are hardly dependent on values of Rm, however; this reason is not clear.

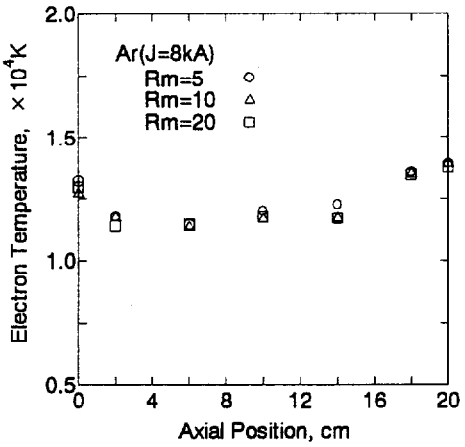

Fig. 4 Axial variations of electron temperatures at the middle of interelectrode at Rm=5~20.

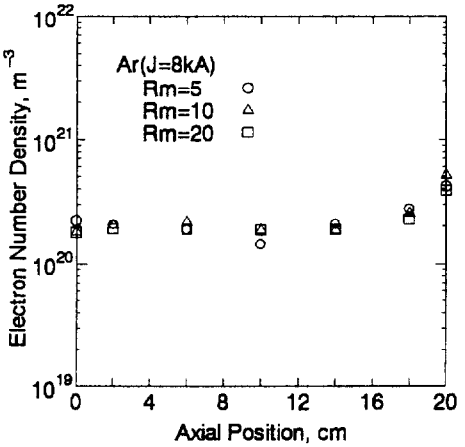

Fig. 5 Axial variations of electron number densities at the middle of interelectrode at Rm=5~20.

Scaling law of MPD channel flowfield

For understanding of the scaling law, current fractions for Ar were measured with the short length MPD channel (MC- II - β) . In order to simplify the discussion, the electrical conductivity is kept constant, if the mass flow rate is same. Therefore, Rm is changed by the discharge current and channel length. Because of testing with the half length of MC- II - α , Rm =2, 5, 10 for MC- II - α are changed to Rm=1, 2.5, 5 for MC- II - β , respectively, with the same mass flow rates. An experiment at Rm=5.9 and 11.3 were conducted at a discharge current of 12 kA and mass flow rates of 0.254 and 0.481 g/sec. Current fractions measured with the short and long length MPD channel are shown in Figs. 6 and 7, respectively, and the horizontal axis in Fig.7 is remade in order to compare to current fractions of MC- II - β ; that is, Figure 2 is modified into current distributions composed of 5 partitions.

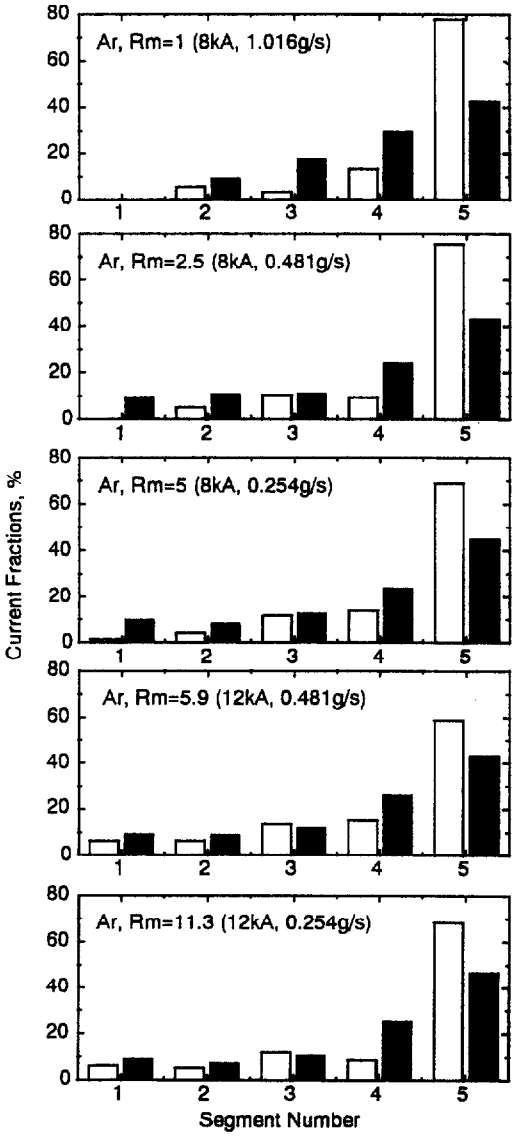

Fig. 6 Current fractions on electrodes for Ar with the short length MPD channel.

As shown in Fig.6, current fractions on the anode drastically concentrate at No. 5 segment at every Rm. On the other hand, those on the cathode gradually increase to the downstream end, and there exists a

little current concentration near the inlet at high Rm. These profiles of current fractions of MC-Ⅱ-β at each Rm roughly agree with those of MC-Ⅱ-α shown in Fig.7, though the channel length, mass flow rate and discharge current were changed. However, current near the inlet for MC-Ⅱ-α concentrates more intensively than that for MC-Ⅱ-β at high Rm. Since the flowfield in the MPD channel contains the real gas effect, a scaling law is not exactly realized, although Kuriki et al.[11] indicated the scaling law of MPD channel flow with the simple magnetoplasmadynamic model, which is ignored of aerodynamic effect; that is, joule heating and chemical reactions were not considered. Hence, the slight differences between the profiles of current fractions for MC-Ⅱ-α and those for MC-Ⅱ-β are appeared. Consequently, it is expected that the scaling law is roughly realized in the MPD channel, when the real gas effect can not be ignored.

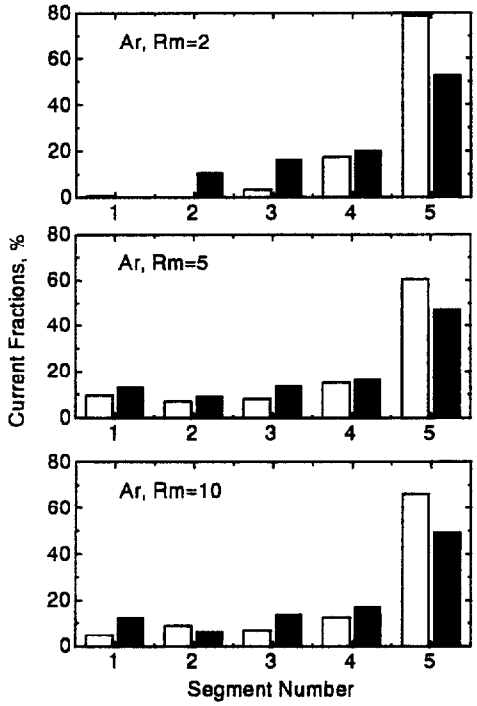

Fig.7 Current fractions on electrodes with the long length MPD channel, which are modified to compare to Fig.2.

One-dimensional Flow Analysis in MPD Channel

One-dimensional model and assumptions

The one-dimensional flowfield analysis[12,13] was conducted to investigate the plasma features and the acceleration processes in the MPD channel. The assumption is as follows.

(1)The gas flows between parallel electrodes.
(2)The flow, electric field and magnetic field are perpendicular to one another.
(3)Viscosity, heat conduction, convection, radiation and Hall effect are neglected.
(4)The electron temperature and the translational temperature of heavy particle species are separated.
(5)Non-equilibrium ionization and dissociation are considered.
(6)The electric field is derived from the choking condition at a sonic point.

In calculation, governing equations are transformed into ordinary differential equations, and the plasma properties are obtained by integrating the ordinary differential equations from the sonic point both upstream to the inlet in the channel and downstream to exit. The boundary conditions at the inlet are predicted from experimented results.

The length and width of the electrodes are 20 and 3.75 π cm, respectively, and the gap between the electrodes is 1.25 cm. The mass flow rates are same as those for the experiments. Plasma properties for Ar at the sonic point are shown in Table.2.

Table 2. Physical Properties at Sonic Point for Ar.

Rm	2	5	10
Electric Field (V/m)	260	377	625
Electron Temp. (K)	12900	14100	17500
Heavy Particle Temp. (K)	310	310	360
Degree of Ionization	0.0012	0.01	0.106

Calculation results and discussion

Figure 8 presents the analyzed distributions of current for Ar at Rm=2, 5, 10. For every Rm, current flows through the channel. As Rm is high, current intensively concentrate near the inlet and outlet. Compared with experimental results, the calculated current distribution at Rm=5 roughly agrees with the experimented one. However, for Rm=2, current does not flow near the upstream end. This is expected because electrical conductivity in the calculation model could not be applied near the inlet. On the other hand, for measured current distribution at Rm=10, there does not exist a intense current concentration near the inlet as shown in Fig.8. Many researchers predict that there exists a strong current concentration near the inlet at high magnetic Reynolds numbers; however, in this experiment, it was not observed. As one of the reasons, it is inferred, from current distributions on the electrodes, that Hall effect was not considered in the calculations.

The electron Hall parameters calculated from results of plasma diagnostic measurement are shown in Fig.9. The electron Hall parameter at Rm=10 is high near the inlet. Accordingly, it is expected that Hall effect have an influence on the flow near the inlet at high magnetic Reynolds number. With strong collisions between particles, Hall effect can be ignored. However, it is inferred that Hall effect can

not be ignored at Rm=10, because mass flow rate is relatively small. Hall effect in an MPD flowfield was predicted from results of numerical analysis and reported in ref.14 and 15.

In addition, electron diffusion may need to be considered. Electrons are easily diffused to the upstream region, because its weight is very light. Therefore, a three fluid model of electron, ion and neutral particles may be required in order to examine an MPD flowfield near the inlet.

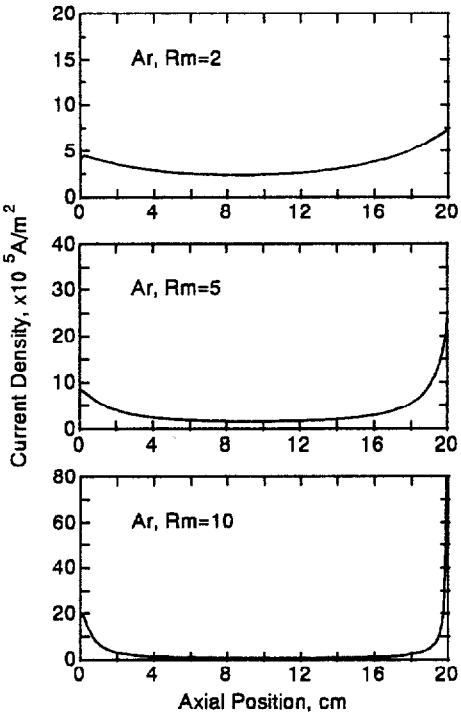

Fig.8 Calculated current distributions at Rm=2~10.

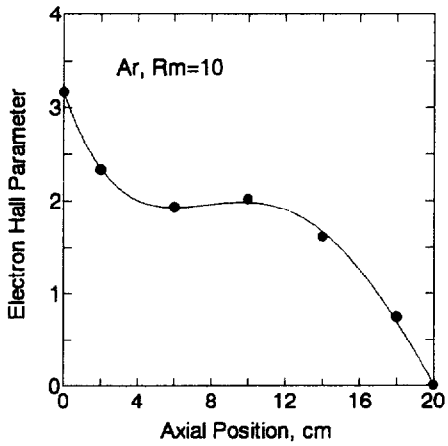

Fig.9 Electron hall parameter estimated from measured plasma parameters at Rm=10.

From comparison to the experimental data, the calculated result at Rm=5 is good agreement with the experimental one. Therefore, the calculated results at Rm=5 are discussed in the following contents. Axial variations of the calculated electron temperature and electron number density are presented in Figs.10 and 11.

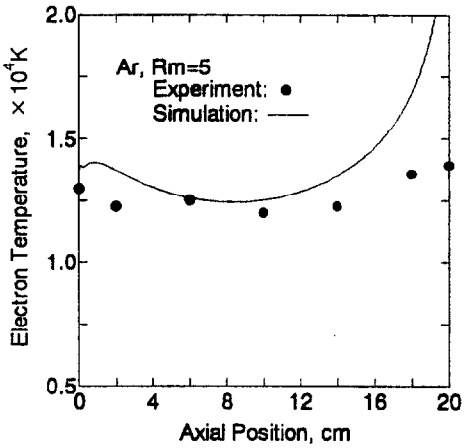

Fig.10 Measured and calculated electron temperature at Rm=5.

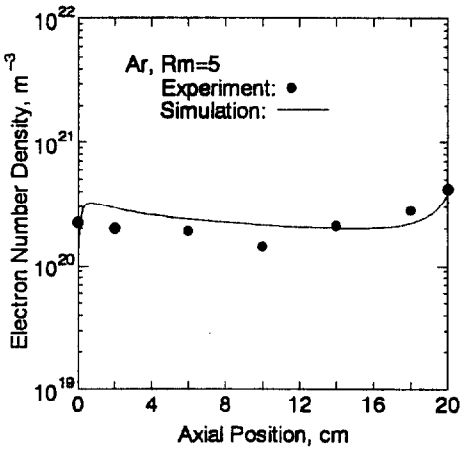

Fig.11 Measured and calculated electron number density at Rm=5.

The calculated electron temperature for Ar is axially kept about 12000 K in the intermediate region and increases near the inlet and outlet, although it disagrees with the measured electron temperature near the exit. From the measured current patterns, current may spread out of the discharge chamber, although in the calculation, current flows only in the chamber. Therefore, since the electron temperature strongly depends on Joule heating, it is inferred that the measured electron temperature near the downstream end differs from the calculated one. Furthermore, this drastic increase in electron temperature near the exit may be because of ignorance of electron heat conduction. The electron number density drastically increases at the inlet and is almost constant in the intermediate region; then it increases near the exit again. This profile agrees

with the measured electron number density for the most part. However, compared with the calculated result, the measured electron number density is relatively large at the inlet, since electron is easily diffused to the upstream region.

The axial variations of the calculated velocity and Mach number for Ar are shown in Fig.12. Plasma is accelerated near the inlet and outlet because of current concentrations. The sonic point is located at 0.075 mm from the upstream end of the MPD channel, and plasma becomes the supersonic flow near the inlet.

As remarked above, the analyzed results for Ar roughly agree with the measured ones at Rm=5. Therefore, it is expected, from the profiles of the calculated plasma velocity and Lorentz force inferred from the measured current distributions on the electrodes, that plasma is accelerated near the inlet and outlet.

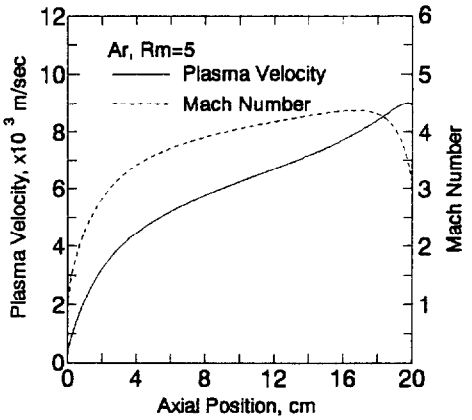

Fig.12 Axial variations of calculated plasma velocity and Mach number at Rm=5.

Acceleration processes in the MPD channel

In order to understand the plasma acceleration processes in detail, the incline of the flow velocity led from governing equations in the one-dimensional flow model is shown below, and the axial distributions of the components of numerators on the right side of the equation are shown in Fig.13.

$$\frac{du}{dx} = \frac{\left(-\frac{2j^2}{5\sigma} + \frac{3}{5} jBu + \frac{2}{5} \rho u R_A \theta_{IA} \frac{d\alpha}{dx} \right) \frac{1}{p}}{M^2 - 1}$$

where x is axial position, u plasma velocity, ρ density, j current density, B magnetic field, α degree of ionization, M Mach number, θ_{IA} characteristic temperature of ionization for Ar atom, R_A gas constant and p gas pressure. The values of K1, K2, K3 in Fig.13 indicate Joule heating, the work by the Lorentz force and the energy density consumed by the ionization process, respectively. K3 means that ionization energy is deprived from the flow; that is, the flow is cooled because of ionization process. Actually, K1 and K3 are substantial heating terms. Hence, K4 (=K1+K3) was also shown in Fig.13, in order to compare electrothermal term with electromagnetic term. K2 is positive in the supersonic flow, so that this works as the component of the acceleration. However, K4 is negative in $M > 1$, therefore K4 works as the component of the deceleration. K4 remains small because of strong ionization near the inlet and outlet, although Joule heating is large in these zones. The absolute value of K2 is larger than that of K4 for the most part except near the inlet and outlet. Accordingly, it is expected from the present numerical analysis that electromagnetic acceleration is dominant in the MPD channel at Rm=5.

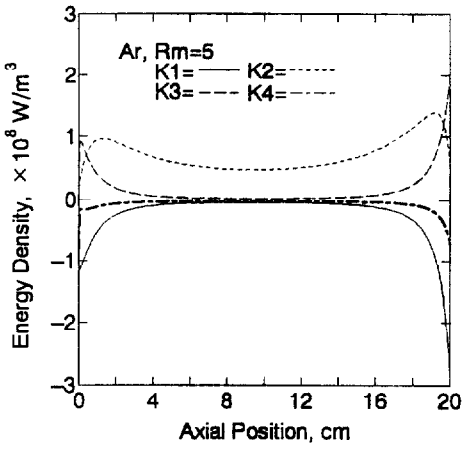

Fig.13 Axial variations of components of energy density deposited in the MPD channel at Rm=5.

The thrust evaluated from the following equation is 4.56 N.

$$Thrust = \dot{m}u_{exit} + Ap_{exit}$$

$$(\dot{m}u_{exit} = 4.30N, \quad Ap_{exit} = 0.26N)$$

The component of the thrust produced by plasma velocity and that by pressure are 4.30 N and 0.26 N, respectively. Consequently, electromagnetic force mainly contributes to the thrust in this operational condition, because, according to discussion of the plasma acceleration mechanism in the MPD channel, plasma is accelerated by electromagnetic force for the most part.

Conclusion

Plasma diagnostic measurement and numerical analysis in a quasi-steady coaxial magnetoplasmadynamic (MPD) channels were made to understand blowing acceleration, i.e., one-dimensional flowfield. For Ar, current fractions on the anode drastically concentrate near the exit, and those on the cathode gradually increase to the outlet.

Furthermore, there exists a slight current concentration near the inlet at high magnetic Reynolds numbers. However, intensive current concentration near the inlet as observed in calculated results does not existed. This is expected because Hall effect has an influence on the MPD flowfield at high Rm. Furthermore, according to comparison measured electron number density with calculated ones, electron diffusion may be required in the calculation model. In the present study, the experiment for confirming the scaling law was also conducted. From the experimental results with different length MPD channels, the profiles of current distributions on the electrodes were roughly determined by Rm, and the scaling law was proved for the most part. According to comparing measured plasma properties for Ar with analyzed ones, experimental results at Rm=5 roughly agree with analytical ones. It is inferred, from profiles of calculated plasma velocity and Lorentz forces estimated from current fractions, that there exist two acceleration zones near the inlet and outlet. Furthermore, it is predicted from the numerical analysis that nonequilibrium ionization process enhanced electromagnetic acceleration through the channel, and electricmagnetic force mainly contributes to the thrust in this condition.

References

1. Toki, K., Shimizu, Y. and Kuriki, K., "An MPD Arcjet Thruster System Test Onboard SFU," 20th Int. Symposium on Space Technology and Science, 96-a-3-13, 1996.

2. Uematsu, K. and Kuriki, K. et al., "Effect of Electrode Configuration on MPD Arcjet Performance," 17th Int. Electric Propulsion Conf.(IEPC), 84-11, 1984.

3. Sovey, J. S. and Mantenieks, M. A., "Performance and Lifetime Assessment of Magnetoplasmadynamic Arc Thruster Technology, J. Propulsion and Power," 7 (1991), pp71-83.

4. Tahara, H., Takiguchi, F., Kagaya, Y. and Yoshikawa, T., "Performance Characteristics and Discharge Features of a Quasi-Steady Applied Field MPD Arcjet," IEPC 91-073, 1991.

5. Tahara, H., Kagaya, Y. and Yoshikawa, T., "Effects of Applied Magnetic Fields on Performance of Quasisteady Magnetoplasmadynamic Arcjet, J.Propulsion and Power," 11(1995), pp.337-342.

6. Wegmann, Th., Auweter-Kurtz, M., Habiger, H. A. and Kurtz, H. L., "Experimental Investigation of Steady State High Power MPD Thrusters," AIAA Paper 92-3464, 1992.

7. Nakayama, T. and Toki, K., "Quantitative Imaging of MPD Flowfield," J. Propulsion and Power, 8(1992), pp. 1217-1223.

8. Mitsuo, K., Tahara, H., Andoh, Y., Kagaya, Y. and Yoshikawa, T., "Arc Structure in a Quasi-Steady MPD Channel," 20th Int. Symposium on Space Technology and Science, 96-a-3-17, 1996.

9. Tahara, H., Yamasaki, N., Mitsuo, K., Kagaya, Y. and Yoshikawa, T., "Plasma Features near Quasisteady Magnetoplasmadynamic Arcjet Cathodes," IEPC 97-118, 1997.

10. Alfvén, H., "Collision between a Non-ionized Gas and a Magnetized Plasma," Rev. Modern Phy., 32(1960), pp.710-713.

11. Kuriki, K., Kunii, Y. and Shimizu, Y., "Idealized Model for Plasma Acceleration in an MHD channel," AIAA Journal, 21(1983), pp.322-326.

12. Lawless, J. L. and Subramaniam, V. V., "Theory of Onset in Magnetoplasmadynamic Thrusters," J. Propulsion and Power, 3(1987), pp.121-127.

13. Shoji, T., Ogiwara, K. and Kimura, I., "Analytical Study on Nonequilibrium Flows in Self-Field MPD Thrusters," IEPC 93-073, 1993.

14. Niewood, E. H. and Martinez-Sanchez, M., "The Hall Effect in a Numerical Model of MPD Thrusters," IEPC 91-099, 1991.

15. Sleziona, P. C., Auweter-Kurtz, M., Schrade, H. O., "Numerical Calculation of a Cylindrical MPD Thruster," IEPC 93-066, 1993.